Nonisothermal Crystallization of Poly(ethylene terephthalate) and Its Blends in the Injection-Molding Process

MASAMI OKAMOTO,* YOSHIHIRO SHINODA, NOBUYUKI KINAMI, and TOMOKO OKUYAMA

Toyobo Research Center, Toyobo Co. Ltd., 1-1 Katata 2-Chome, Ohtsu, Shiga 520-02, Japan

SYNOPSIS

We investigated the nonisothermal crystallization during the cooling process of injection molding of poly(ethylene terephthalate) (PET), PET/talc, and PET/Surlyn blends. We applied the isothermal crystallization parameters obtained by the Hoffman–Lauritzen theory to the kinetics of nonisothermal crystallization and then calculated the relative crystallinity χ/χ_c as a function of the mold temperature. χ/χ_c were nicely interpreted by calculation without effect of the pressure history on crystallization in PET and PET/talc (1 wt %) blends. In contrast, in the PET/Surlyn (3 wt %) blend, crystallization occurred at a lower mold temperature than predicted by our calculation. The transmission electron micrograph near the surface of the injection-molded PET/Surlyn blend showed deformation and stretching of dispersed Surlyn particles, suggesting that orientation of the PET matrix proceeds with the flow in processing. The orientation of the PET matrix resulted in acceleration of the crystallization in the injection molding. © 1995 John Wiley & Sons, Inc.

INTRODUCTION

Injection molding for semicrystalline polymers involves a complicated thermal history and stress field, i.e., a nonisothermal cooling process, stress during injection pressure loading, and simultaneous orientation of molecular chains. In this situation, the key to material design is careful control of processing conditions. Ten years ago, there were considerable experiments and simulation to investigate the mold-filling and cooling effects of amorphous polymers.[1-3] Kamal discussed the ultimate degree of crystallinity by combining heat transfer and kinetics of crystallization models. Rgdahl proposed inclusion of the estimation of the residual stress distribution into the calculated procedure.[4]

Recently, computer aided engineering (CAE) has been a powerful tool for investigating process analysis. With this, it is possible to predict mold shrinkage and warpage due to the crystallization; however, it is difficult to practically estimate actual volume change during molding so that the simulated results are strongly dependent on the many parameters set.[5] To understand the crystallization in injection molding, it is very important to measure the transient temperature, pressure, and crystallization behavior during the cooling process.[6] A preliminary study was carried out, in our previous article, under isothermal crystallization conditions on processing ability as a function of mold temperature in the case of a poly(ethylene terephthalate) (PET)/talc system.[7]

In this article, we extend the study of the nonisothermal crystallization of PET, PET/talc, and PET/polyethylene ionomer blends, taking into account not only pressure but also orientation during injection molding. Furthermore, we measure the actual transient resin temperature and loading pressure in the mold and apply the isothermal crystallization parameters obtained by the Hoffman–Lauritzen theory to the kinetics of nonisothermal crystallization and calculate the degree of crystallinity as a function of the various mold temperatures during cooling. We discuss, in detail, the nonisothermal crystallization behavior of the polymer blends in the injection molding.

* To whom correspondence should be addressed.

Journal of Applied Polymer Science, Vol. 57, 1055–1061 (1995)
 CCC 0021-8995/95/091055-07

EXPERIMENTAL

Poly(ethylene terephthalate) (PET) used in this study was a commercial product from Toyobo Co. (RE530, $M_w = 4.6 \times 10^4$; Toyobo Plastic Division). The talc was generously supplied by the Hayashi Kasei Co. (talkan-PK, mean diameter = 8.0 μm) and the polyethylene ionomer was from DuPont (Surlyn #1707, sodium-neutralized acrylicacid ~ 3 wt %). Mixtures of PET/talc (1 wt %) and PET/Surlyn (3 wt %) were melt mixed in a corotating twin extruder (Ikegai Machinery Co.; 30 mm ϕ, L/D = 16; barrel temperature = 280–290°C). The extruded melt was quickly quenched into ice water and chopped into pellets. The pellets were injection molded to a sheet ($30 \times 100 \times 1$ mm) by an injection machine (Toshiba Machinery Co., IS-100; barrel temp. = 280°C, injection time = 10 s, holding time = 20 s) at various mold temperatures. Injection speed was 5.2 cm^3/s, which corresponded to a low speed. During the melt-cooling process, just after the mold filled, the resin temperature and loading pressure were monitored by embedding the thermocouple and pressure sensor in the mold. The injection-molded specimen was mounted on an ultramicrotome (Ultracut N, Reichert-Jung) and microtomed to provide a flat specimen (~ 50 μm) from the surface, and the degree of crystallinity χ_c was measured. χ_c was measured by a Perkin–Elmer differential scanning calorimeter (d.s.c.), DSC-7 at a heating rate of 20°C/min with indium as a calibration standard. We estimated χ_c using the endothermic peak at the melting point of the microtomed thin specimen, taking into account the exothermic peak during the heating process due to the incompletely crystallized specimens. That is, χ_c of each microtomed specimen was determined from:

$$\chi_c(\text{wt \%}) = \Delta H / \Delta H^\circ \qquad (1)$$

where $\Delta H = \Delta H_{\text{melting}} - \Delta H_{\text{heating process}}$ and ΔH° is the heat of fusion of 100% crystalline PET (ΔH° = 122 J/g).[8] We also measured the nonisothermal crystallization behavior during the cooling process of extruded-and-quenched blends and neat PET by d.s.c. at various cooling rates.

For the analysis of the isothermal crystallization behavior, the quenched blends and PET were placed between two cover glasses and melt pressed to a thin film (ca. 20 μm thick) at 280°C ($> T_m$ of PET) for 1 min. Then the remelt underwent a rapid temperature-drop to the various isothermal crystallization temperatures by putting it on a hot stage set on a light-scattering apparatus. Immediately after the temperature drop, the time-resolved light-scattering measurement was carried out as described in the previous articles.[7,9] The radiation of a polarized He–Ne laser of 632.8 nm wave length λ was applied vertically to the film specimen and the scattering profile was observed at an azimuthal angle of 45° under Hv (crosspolarized) optical alignment.

The morphology of the injection-molded specimen was observed under transmission electron microscopy (TEM), using a Hitachi H-600 (100 kV) with a microtomed-thin section (ca. 70 nm) with ruthenium tetroxide staining.

To understand the nonisothermal crystallization in a complex stress field, we carried out the pressure–temperature–volume (PVT) measurement by a PVT apparatus from Shimazu (PVT-200). The cell was filled with quenched blend or neat PET with approximately 1 g of polymer and mercury. The cell was closed on one end by a flexible bellows and the expansion was measured with changing temperature in order to determine the volume at a cooling rate of 10°C/min and loading pressure range of 1 to 50 MPa.

The orientation at the surface of an injection-molded specimen was analyzed qualitatively by chain-intrinsic fluorescence intensity.[10] The measurements were carried out using a fluorescence spectrophotometer Hitachi F-4010. The excited wavelength around 340 nm had an angle of 70° to the injection-molded specimen surface. The emission spectrum then had a maximum around 390 nm. Using polarized-incident light and measuring the polarized components of the fluorescent light, we estimated the degree of orientation of the fluorescent intensity between the flow direction and the cross-flow one.

RESULTS AND DISCUSSION

Isothermal Crystallization Kinetics

In order to estimate the nonisothermal crystallization during the cooling process in injection molding, it is necessary to know the isothermal crystallization behavior of the blends and neat PET. Light scattering is a powerful and very convenient tool to determine the crystallization kinetics.[11,12]

The change of the Hv light-scattering patterns during isothermal crystallization at various temperatures ranging from 110 to 240°C were studied, and we obtained a four-leaf clover pattern at an early stage of crystallization, suggesting that spherulites are formed and then grow with time. From the one-dimensional Hv scattering profiles at an azimuthal

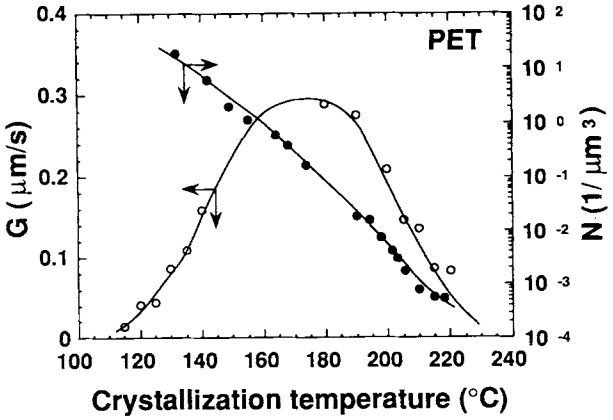

Figure 1 Temperature dependence of G and N in isothermal crystallization of PET.

angle 45° in the scattering patterns at various crystallization times, one can obtain the average radius of spherulites R_{Hv} by a maximum at scattering angle θ_m[11]

$$4.09 = 4\pi(R_{Hv}/\lambda)\sin(\theta_m/2) \quad (2)$$

Time variation of the radius of the spherulite R_{Hv}, at various crystallization temperatures T_c, was obtained, and R_{Hv} showed a linear growth. From the slope, the linear growth rate of the spherulite G ($= dR_{Hv}/dt$) was obtained and is shown in Figure 1. Using the crude approximation that all the spherulites were of identical size, the primary nucleation density of the spherulites, i.e., the number of heterogeneous nuclei N, was estimated by:

$$N = (3/4\pi)R_m^{-3} \quad (3)$$

where R_m is the maximum radius of the spherulite, i.e., the attainable radius before impingement. The crystallization temperature dependence of N is shown in Figure 1.

It is generally accepted that the growth rate of spherulites may be expressed by the Hoffman–Lauritzen theory[13,14]

$$G = G_0 \exp[-U^*/R(T_c - T_g + 30)]\exp[-K_g/T_c(\Delta T)f] \quad (4)$$

where U^* is the transport activation energy for chain diffusion, R is the gas constant, K_g is the nucleation constant for secondary nucleation, ΔT is the supercooling ($= T_m^\circ - T_c$, T_m° being the equilibrium melting temperature and T_c being the crystallization temperature), and f is the correction factor given by $2T_c/(T_m^\circ + T_c)$. The nucleation constant K_g is given by:

$$K_g = nb\sigma\sigma_e T_m^\circ/\Delta H^\circ k \quad (5)$$

where b is the thickness of a monomolecular layer comprising the perpendicular separation of (010) planes (i.e., $b = 5.53$ Å),[15] σ and σ_e are the lateral and end-surface free energies, respectively, k is the Boltzmann constant, and n takes on a value of 4 in regime I or III and a value of 2 in regime II. The equilibrium melting point of each sample was determined from a Hoffman–Weeks plot for the isothermally crystallized sample (10 h crystallization).[7,9]

Assuming heterogeneous nucleation with concurrent three-dimensional growth, then the number of nuclei N is given by:[16]

$$N = N_0 \exp[-aT_m^\circ/T_c(\Delta T)f] \quad (6)$$

where a is constant.

Using the eqs. (4) to (6), one can estimate the unknown parameters for each blend and neat PET. All parameters thus obtained are listed in Table I.

Nonisothermal Crystallization Kinetics

Because rapid cooling occurs in the injection-molding process, we have to take this situation into account and use nonisothermal crystallization kinetics. Figure 2 shows the preliminary results of the temperature dependence of the reduced degree of crystallinity χ/χ_c from the melt state at various cooling

Table I Characteristic Parameters Obtained from Eqs. (4) to (6)

Sample	T_m° (°C)	U* (cal/mol)	$\sigma\sigma_e \times 10^{-5}$ (cal²/m⁴)	$G_0 \times 10^{-4}$ (μm/s)	T_{tr}^a (°C)	$N_0 \times 10^{-3}$ (μm⁻³)	$a \times 10^{-2}$ (K⁻¹)
PET	279	1384	2.85	3.2	202	8.1	6.25
PET/talc (1 wt %)	279	1380	2.80	3.2	202	13.4	6.4
PET/Surlyn (3 wt %)	279	1273	2.57	3.0	207	22.0	7.5

[a] Regime transition temperature from II to III.

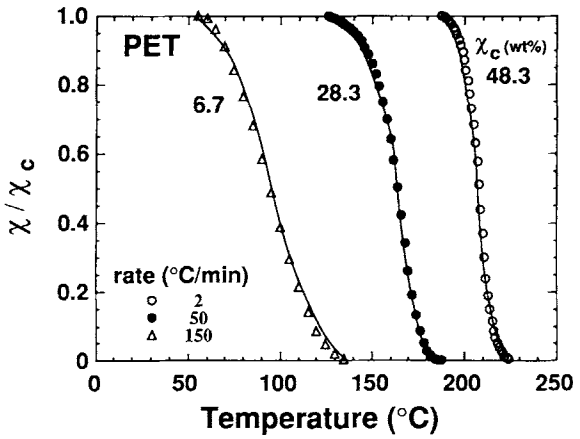

Figure 2 Nonisothermal crystallization behavior of PET at various cooling rates.

rates of neat PET measured by d.s.c. Slow crystallization is observed with increasing cooling rate, i.e., high cooling rate disturbs the nonisothermal crystallization.

According to Avrami[17,18] and Mandelkern,[19] the time dependence of χ_c for the nonisothermal process under certain assumptions is given by:

$$-\ln\left(1-\frac{\chi}{\chi_c}\right) = \frac{1}{\chi_c}\frac{\rho_c}{\rho_l}\int_0^t \left\{\int_{t_s^*}^t G(u)du\right\}^m N(t^*)dt_s^* \quad (7)$$

where ρ_c and ρ_l are the density of the crystalline and liquid phase, respectively, t_s^* is the initiation time of crystallization, and m is the shape factor constant (= 3, three-dimensional growth). t_s^* is also related to the initiation temperature T^* or T_s^* (in injection molding) of crystallization after a temperature drop, which is discussed later.

Using eq. (7) and t_s^* (or T^*), one can calculate the temperature dependence of χ/χ_c. The solid lines in Figure 2 are calculated profiles, and one can see good agreement between experimental and calculated results. The nonisothermal crystallizaton behavior is nicely reproduced here by calculation.

Analysis of the Injection-Molding Process

Typical experimental data relating to the time variations of the resin temperature and loading pressure at the mold wall during the cooling process of neat PET, just after the filling stage, are shown in Figure 3. A large pressure is applied to the polymer liquid at an early stage in the cooling process ($t \leq 4$ s) and then the pressure is decreased rapidly with time and finally is close to zero for 12 s. The resin temperature profiles at various mold-temperature conditions indicate that rapid cooling occurs at the mold surface as expected, and polymer is fixed at the initial setting mold temperature for more than 12 s. The question is, when dose the crystallization start during the cooling stage? If the crystallization starts in the temperature range from 220 to 170°C, one should take into account the effect of the pressure on crystallization. That is, the crystallization will be accelerated several orders of magnitude and change the dimensionality of the crystal growth such as shish-kebab.

In contrast, crystallization at a late stage of the cooling process may be close to the quiescent state, except for the molecular orientation. To confirm the above point, we estimated the initiation temperature T_s^* during nonisothermal crystallization in the injection-molding process as follows. The cooling rate dependence of T^*, measured by d.s.c., of each blend and neat PET are shown in Figure 4. In the case of neat PET, no crystallization occurs more with than a 300°C/min cooling rate because T^* is below T_g ($\sim$ 78°C). Combining the results in Figures 3 and 4, one can estimate T_s^* as a crossover point between cooling profiles in the injection-molding process and T^* profile as a function of cooling rate again in Figure 5. One can see a rapid cooling of molten polymer at an early stage of the cooling process (more than 1000°C/min). Note that T_s^* corresponds to the late stage of the cooling process, i.e., the effect of pressure may be negligible on crystallization, and no crystallization occurs at low mold temperature ($\sim$ 50°C), because T_s^* is below T_g. Figure 6 shows the typical PVT result for a PET/talc blend. At high

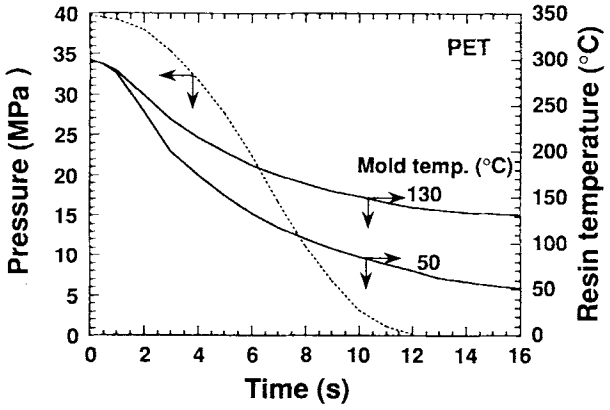

Figure 3 Change of pressure and resin temperature profiles during the cooling process just after the filling stage.

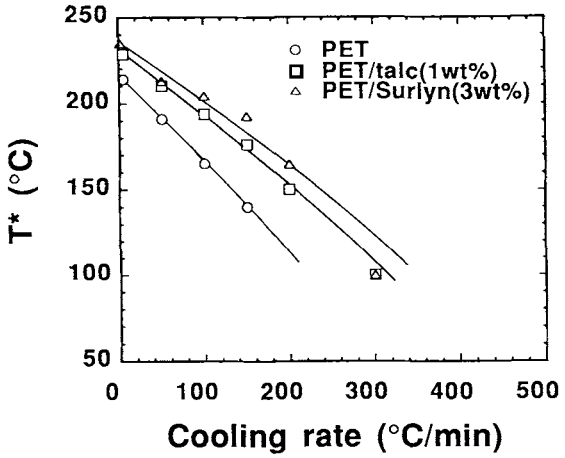

Figure 4 Cooling rate dependence of T^*.

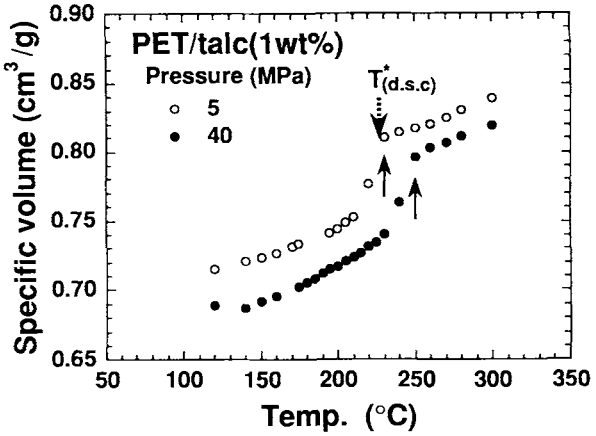

Figure 6 PVT data for the PET/talc (1 wt %) blend.

loading pressure, T^* (indicating arrow in Fig. 6) goes up to a higher temperature due to the entropy loss in the case of 40 MPa. The decrease in entropy of the polymer melt allows crystallization to occur at a higher temperature than would normally be observed without deformation. However, at low pressure ($\leq$ 5 MPa), there is no difference and no accelerated behavior of crystallization during the cooling process compared with the quiescent state T^* obtained by d.s.c. In each blend and PET, we believe the effect of the pressure is negligible.

Now, having obtained T_s^*, we use our simulation work to predict the nonisothermal crystallization in injection molding. Figure 7 shows the crystallinity χ_c obtained from the injection-molding experiment and the calculated relative crystallinity χ/χ_c at various mold temperatures. The solid and two dashed lines are calculated results using the nonisothermal kinetics model [eq. (7)], T_s^*, and crystallization parameters in Table I. One sees a slight deviation between calculation and experiment; however, the predictions of neat PET and the PET/talc blend show that the nonisothermal model can predict χ_c well. Note that the simulation avoids complications resulting from the effect of pressure and shear on crystallization kinetics. The small deviation may be an effect of the molecular orientation due to the fast flow in the cold cavity near the wall.

On the other hand, a big difference is seen in the accelerated PET/Surlyn blend, suggesting that, in this case, the shear and orientation induced crystallization kinetics because the melt viscosity of the PET/Surlyn blend increases compared with neat PET and the PET/talc blend. It is well known that orientation accelerates crystallization, particularly at higher melt viscosity.[20,21]

Furthermore, we carried out the analysis of the surface of the injection-molding specimen to clarify

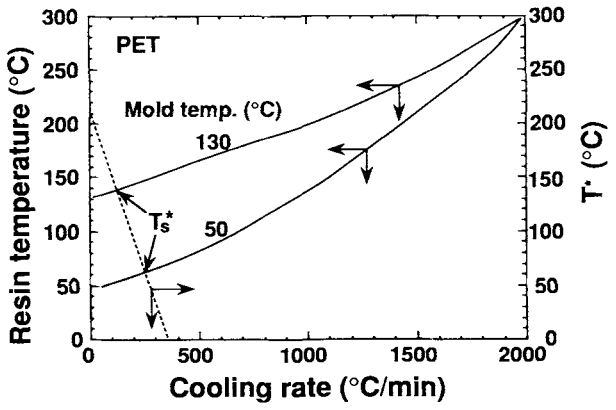

Figure 5 Plots of resin temperature and T^* against cooling rate for PET.

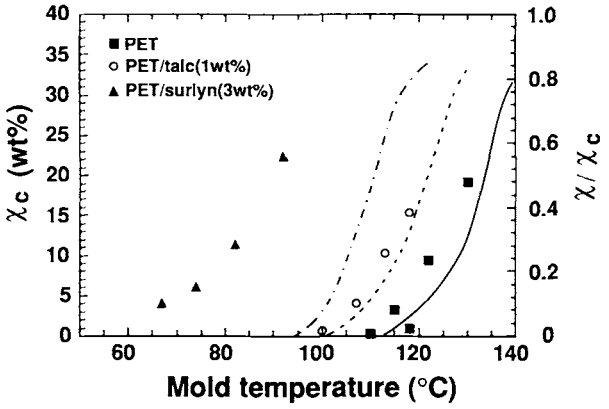

Figure 7 Variation of χ_c with mold temperature in injection molding and calculated relative crystallinity χ/χ_c. Calculated value (—) in PET, (----) in PET/talc (1 wt %), and (— - —) in PET/Surlyn (3 wt %) (injection = 10 s + holding = 20 s).

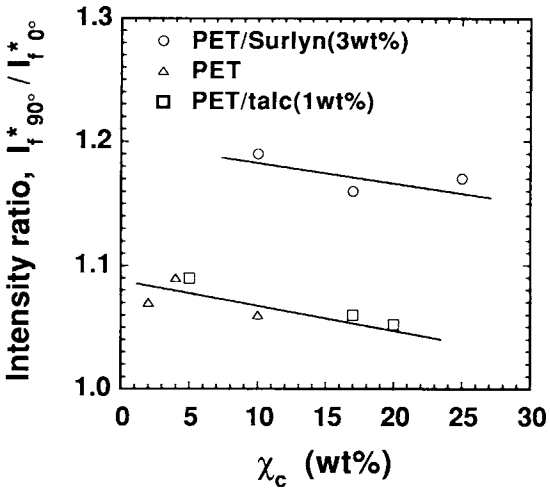

Figure 8 Fluorescence intensities vs. χ_c.

the orientation with the flow. The chain-intrinsic fluoresence intensity around 390 nm is related to the degree of amorphous orientation.[10] The intensity ratio between the flow direction $I_f^*0°$ and a crossflow one $I_f^*90°$ provide the orientation behavior at the surface of the injection-molded specimen. Figure 8 shows the fluorescent properties of each blend and PET as a function of χ_c as molded. In the PET/Surlyn blend, one sees a higher level of intensity ratio, suggesting that the big difference arises from enhanced orientation. The orientation proceeds more so at the surface of the injection-molded specimen.

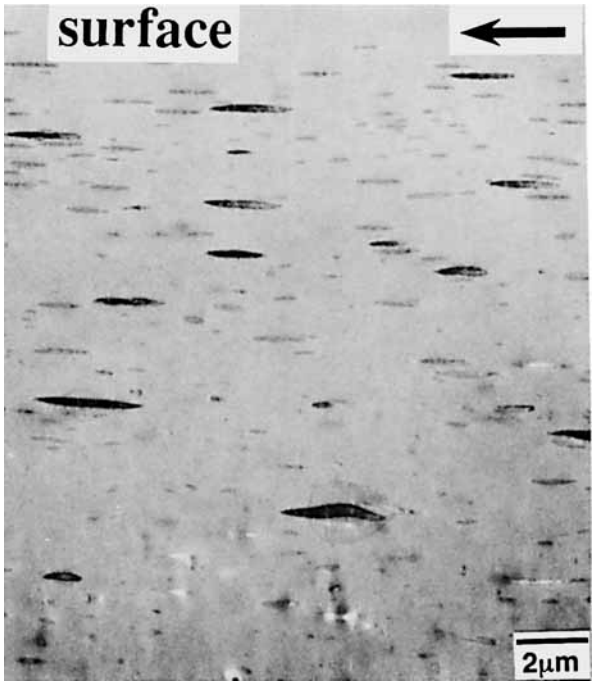

Figure 9 Transmission electron micrograph (RuO_4) of the PET/Surlyn (3 wt %) near the surface of an injection-molded specimen. Arrow indicates flow direction.

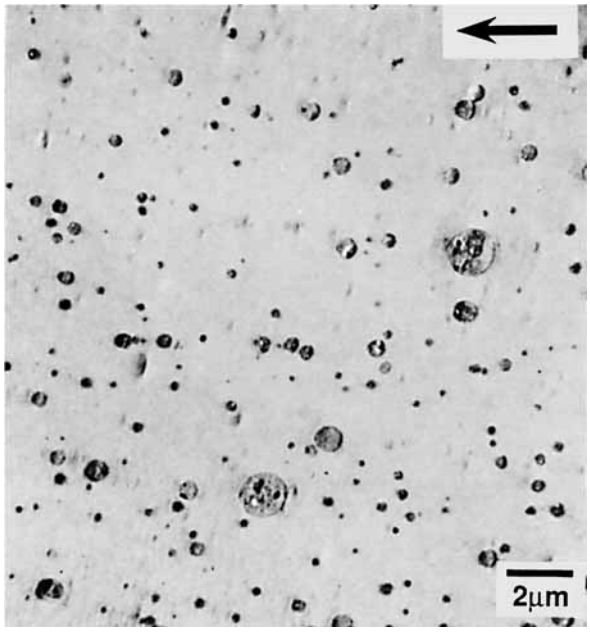

Figure 10 Transmission electron micrograph (RuO_4) of the PET/Surlyn (3 wt %) at the center of an injection-molded specimen. Arrow indicates flow direction.

Figure 9 is a TEM photograph of the PET/Surlyn blend near the surface in the flow direction. As expected from Figures 7 and 8, one can see the large deformation and orientation of dispersed Surlyn particles. The average diameter of the dispersed particles near the center of the specimen is ca. 0.5 μm, as shown in Figure 10. That is, the Surlyn particles near the surface are stretched four times with the flow. Thus, the orientation may result in acceleration of the crystallization in injection molding.

CONCLUSION

In the slow crystallizing of the PET/talc blend and neat PET, nonisothermal crystallization during the cooling process in injection molding can be used to successfully predict the nonisothermal kinetics with the effect of the pressure. This implies that the crystallization starts in the negligibly small loading pressure regime and late stage of the cooling process. It is found that in the PET/Surlyn blend, very significantly orientation occurs near the surface so that the crystallization is accelerated in spite of a

low mold temperature. It is necessary to understand experimentally the effect of shear stress and orientation on nonisothermal crystallization kinetics quantitatively. This subject is currently being followed up in our laboratories.

REFERENCES

1. W. Dietz, J. L. White, and E. S. Clark, *Polym. Eng. Sci.*, **18,** 273 (1978).
2. M. R. Kamal and V. Tan, *Polym. Eng. Sci.*, **19,** 558 (1979).
3. G. Marruci, *Rheol. Acta,* **12,** 269 (1973).
4. M. Rigdahl, *Int. J. Polym. Mater.*, **5,** 43 (1976).
5. L. T. Manzione, *Applications of Aided Engineering in Injection Molding,* Hanser, Munich, 1987.
6. J. D. Muzzy, D. G. Bright, and G. H. Hoyos, *Polym. Eng. Sci.*, **18,** 437 (1978).
7. Y. Shinoda, T. Okuyama, and M. Okamoto, *Seikei Kakou,* **5,** 481, (1993).
8. B. Wunderlich, *Macromolecular Physics,* Vol. 3, Academic Press, New York, 1980.
9. M. Okamoto and T. Inoue, *Polymer,* to appear.
10. B. Clauss and D. R. Salem, *Polymer,* **33,** 3193 (1992).
11. R. S. Stein and M. B. Rhodes, *J. Appl. Phys.*, **31,** 1873, (1960).
12. C. H. Lee, H. Saito, and T. Inoue, *Macromolecules,* **26,** 6566 (1993).
13. J. D. Hoffman and J. I. Lauritzen, *J. Res. Natl. Bur. Stand.*, **(A)65,** 279 (1961).
14. J. D. Hoffman, G. T. Davis, and J. I. Lauritzen, *Treatise on Solid-State Chemistry,* Vol. 3, N. B. Hanny, Ed., Plenum Press, New York, 1976.
15. L. H. Pals and P. J. Phillips, *J. Polym. Sci., Polym. Phys. Ed.*, **18,** 829 (1980).
16. H. Ito, K. Minagawa, K. Koyama, and H. Takeda, *Polym. Prepr. Jpn.*, **43,** 1648 (1994).
17. M. Avrami, *J. Chem. Phys.*, **7,** 1103 (1939).
18. M. Avrami, *J. Chem. Phys.*, **8,** 212 (1940).
19. L. Mandelkern, *Crystallization of Polymers,* McGraw-Hill, New York, 1964.
20. G. C. Alfonso, M. P. Verdona, and A. Wasiak, *Polymer,* **19,** 711 (1978).
21. O. Ishizuka and K. Koyama, *Polymer,* **28,** 913 (1977).

Received January 12, 1995
Accepted February 6, 1995